Soft Matter

Accepted Manuscript

This article can be cited before page numbers have been issued, to do this please use: H. Shih, C. Hsieh, M. G. Mohamed, C. Y. Zhu and S. Kuo, *Soft Matter*, 2015, DOI: 10.1039/C5SM02569A.

ROYAL SOCIETY OF CHEMISTRY

www.rsc.org/softmatter

View Article Online
DOI: 10.1039/C5SM02569A

Ternary Polybenzoxazine/POSS/SWCNT Hybrid Nanocomposites Stabilized through Supramolecular Interactions

Hsi-Kang Shih,[a] Chun-Cheng Hsieh,[b] Mohamed Gamal Mohamed,[b] Chao-Yuan Zhu[a,*] and Shiao-Wei Kuo[b,*]

Received (in XXX, XXX) Xth XXXXXXXXX 200X, Accepted Xth XXXXXXXXX 200X
DOI: 10.1039/b000000x

In this study we linked zero-dimensional polyhedral oligomeric silsesquioxane (POSS) with one-dimensional single-walled carbon nanotubes (SWCNTs) as dual-dimensional nanohybrid complexes within polybenzoxazine matrices, stabilized through noncovalent supramolecular interactions. First, we synthesized a new bifunctionalized benzoxazine (Py-Bz-T), presenting thymine (T) and pyrene (Py) units, that displayed excellent thermal properties after thermal curing, because its T moieties increased the physical cross-linking density. Second, we prepared Py-Bz-T/OBA-POSS [octuply adenine (A)-functionalized POSS] nanocomposites and investigated, using nuclear magnetic resonance and Fourier transform infrared spectroscopies, the multiple hydrogen bonding A···T interactions between Py-Bz-T and OBA-POSS. Finally, we prepared Py-Bz-T/OBA-POSS/SWCNT ternary hybrid complexes dispersed in THF, stabilized through both multiple hydrogen bonding and π–π stacking interactions. Transmission electron microscopy revealed that the SWCNTs were highly dispersed and covered by the Py-Bz-T/OBA-POSS nanocomposites; these ternary hybrid complexes were stabilized through π–π interactions between Py-Bz-T/OBA-POSS and the SWCNTs, as evidenced using fluorescence spectroscopy.

Introduction

Since the first developments in benzoxazine chemistry in the 1940s, their polymerization to form polybenzoxazines through thermal activation has been investigated in great depth.[1–4] Benzoxazine monomers are generally synthesized through Mannich reactions from primary amines, phenol-based compounds, and formaldehyde that construct the heterocyclic oxazine ring. As a result, benzoxazine monomers have great structural flexibility in terms of their molecular design and have a variety of applications.[5–9] Polybenzoxazines have several outstanding characteristics, including no requirement for a catalyst in the polymerization process, tunable glass transition temperatures (T_g), high flame retardance, excellent mechanical performance, and low surface free energies.[10–18]

Self-assembly of supramolecular materials has drawn great attention, taking advantage of new structural organizations formed through highly complementary molecular recognition events.[19–23] Supramolecular interactions, mediated through noncovalent bonding (namely electrostatic, hydrogen bonding, metal–ligand, and π–π interactions), are powerful tools for preparing many complex molecular architectures.[24–26] Through tailoring of appropriate functional groups, we can exploit different supramolecular interactions—offering different strengths, binding kinetics, and directionalities—for desired purposes. For example, DNA and RNA sequences, which use supramolecular chemistry to store, transmit, and replicate information in biological environments, also offer the opportunity to prepare unnatural controlled self-assembled architectures.[27] Meijer *et al.* has introduced several supramolecular structures into polymers or polymerization processes to form novel materials with specific physical and mechanical properties.[19, 28–31] Supramolecular materials generally respond to changes in their environment (*e.g.*, pH, light, temperature, electric field), allowing ready control over the strength and selectivity of their interactions. The transcription and translation of DNA are excellent instances of the assembly and disassembly of supramolecular strutures.[32] By exploiting such interactions, we can also construct polymers through the linking of monomers or functionalized side chains of polymer networks that are capable of noncovalent bonding—an attractive approach toward establishing "smart" (stimuli-responsive) soft materials.[19, 33]

Research in supramolecular chemistry, using, for example, crown ethers, spherands, and carcerands, takes its inspiration from the field of both chemistry and biology.[34–36] Many synthetic binding motifs have been developed to orient guest molecule within host molecules through specific interactions.[37–43] An increased number of hydrogen bonds will generally increase the stability (measured in terms of the association constant) of an assembled complex, as evidenced by the association constant of the G···C complex in DNA being two to three orders of magnitude higher than that of the A···T complex. In addition to the enthalpy of intermolecular hydrogen bonds, association constants are also affected by the enthalpy of intramolecular hydrogen bonds, preorganization,[44] the arrangement of interacting groups,[45, 46] and tautomerization.[47, 48]

The properties of polymers can be improved upon blending with inorganic nano-fillers, which may have spherical (fullerenes, semi-conductive nanoparticles), fibrous [carbon nanotubes (CNTs), metal nanowires], or layered (clay, graphene) structures. Polyhedral oligomeric silsesquioxane (POSS) has been studied as a zero-dimensional nano-filler for many years.[49–52] Derivatives of POSS $(RSi_2O_3)_n$ have been developed with values of n of 2, 3, 4, 5, and 6 (named T_4, T_6, T_8, T_{10}, and T_{12}, respectively), with R groups as hydrogen atoms and alkyl, alcohol, amine, epoxide, and aryl units.[53] Two main kinds of T_8-POSS are commonly applied: one with eight reactive functional groups and the other selectively functionalized with seven inert organic hydrocarbon units and one reactive functional group.[54–56] The attractions of using POSS derivatives relative to other nano-fillers are their well-defined molecular structures, monodisperse molecular weights, low densities, excellent temperature-stabilities, and high structural flexibility in terms of molecular design. CNTs, discovered in

[a]Institute of Applied Chemistry, National Chiao Tung University, HsinChu, 300 Taiwan
E-mail: cyzhu@mail.nctu.edu.tw
[b]Department of Materials and Optoelectronic Science, Center for Nanoscience and Nanotechnology, National Sun Yat-Sen University, Kaohsiung, 804, Taiwan.
E-mail: kuosw@faculty.nsysu.edu.tw

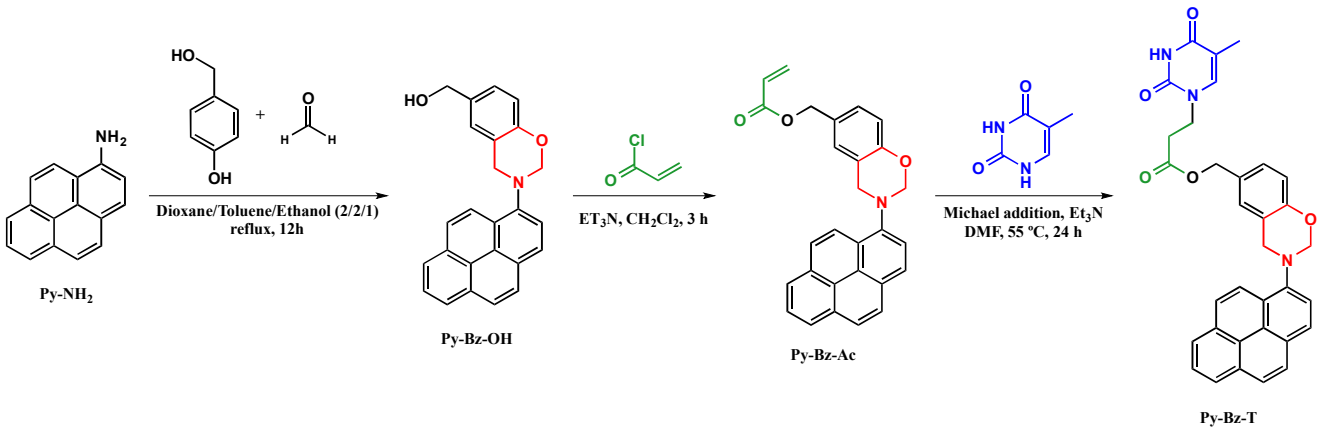

Scheme 1 Synthesis of Py-Bz-T.

1991,[57] are highly applicable in both materials and life sciences[58–63] because of their one-dimensional nanostructures and excellent thermal,[64–66] electronic,[67] optical,[68] and mechanical[69] properties. CNTs are formed as disordered powders in highly entangled states, with their individual nanotubes interacting through van der Waals forces. Accordingly, they have low dispersibility or solubility in organic solvents and are difficult to process, limiting the variety of their applications. Covalent (chemical) functionalization is a promising means of improving the dispersibility and reactivity of CNTs. Several methods have been tested to modify the surfaces of CNTs through chemical treatment, including "grafting-from" (functionalizing as initiators for grafting of polymers)[70–72] and oxidation at defect sites.[73, 74] Such chemical functionalization, however, changes the sp^2 hybridization of some of the carbon atoms of the CNTs to sp^3 hybridization, possibly deteriorating their thermal, electronic, optical, and mechanical properties. Unlike chemical functionalization, noncovalent functionalization using multi-aromatic systems can enhance the dispersibility of CNTs while maintaining their electronic configuration. Because pyrene (Py) interacts with CNTs in a manner similar to the interactions among CNTs, many polymers have been synthesized with Py units to investigate their potential to enhance the dispersion of CNTs.

Hybrid nanomaterials with multidimensional structures can be attractive materials because of their unique physical properties, specific structures, and variety of applications.[75–82] In this present study, we examined the combination of a zero-dimensional nanostructure (POSS) with a one-dimensional nanostructure [single-walled CNTs (SWCNTs)], stabilized through supramolecular interactions. We synthesized a new benzoxazine derivative, Py-Bz-T, bifunctionalized with thymine (T) and Py units (Scheme 1). Using differential scanning calorimetry (DSC) and Fourier transform infrared (FTIR) spectroscopy, we investigated the curing behavior of Py-Bz-T. We found that Py-Bz-T was readily polymerized upon heating at 200 °C for 1 h, with the cured-Py-Bz-T displaying excellent thermal properties because its T functional groups increased the physical cross-linking density. Meanwhile, we also synthesized and characterized an octuply adenine (A)-functionalized POSS derivative (OBA-POSS). We used nuclear magnetic resonance (NMR) and FTIR spectroscopy to analyze the multiple hydrogen bonding interactions in the resulting Py-Bz-T/OBA-POSS nanocomposites. Furthermore, we prepared ternary Py-Bz-T/OBA-POSS/SWCNT hybrid complexes and used fluorescence spectroscopy and transmission electron microscopy (TEM) to investigate their dispersity and optical properties.

Experimental Section

Materials and Characterization

Chemical reagents were purchased from Hybrid Plastics, Alfa Aesar, or Aldrich (USA) and used without purification. All solvents were purchased from Tedia (USA) and distilled over CaH_2 prior to use. SWCNTs were obtained from Centron Biochemistry Technology and used without purification. Pyren-1-amine and OBA-POSS were prepared according to previously reported procedures;[83, 84] characterization data in provided in the Supplementary Information. ^{13}C and ^{1}H NMR spectra were recorded using a Varian Inova 500 Instrument (standard solvents: d_6-DMSO and d_2-1,1,2,2-tetrachloroethane); chemical shifts are reported in parts per million (ppm). The concentration for NMR spectra is 10 mg/ml. A Bruker Tensor 27 apparatus was used to record FTIR spectra (conventional KBr disk method; 32 scans; resolution: 1 cm^{-1}). Dynamic curing kinetics and glass transition temperatures were measured using a TA Q-20 differential scanning calorimeter (sample weight: ca. 5-7 mg; sealed aluminum sample pan), operated under a N_2 atmosphere with a flow rate of 50 mL min^{-1} (temperature range: 10–310 °C; heating rate: 20 °C min^{-1}). Thermal stability was measured using a TA Q-50 thermogravimetric analyzer, operated under a N_2 atmosphere at a flow rate of 60 mL min^{-1} (temperature range: 35–800 °C; heating rate: 20 °C min^{-1}; sample weight: ca. 5–7 mg; Pt cell). Fluorescence and UV–Vis spectra were recorded using a Hitachi F4500 luminescence spectrometer and an HP 8453 diode-array spectrophotometer. Dynamic mechanical analysis (DMA) was performed using a PerkinElmer Instruments DMA 8000 apparatus operated over a temperature range from 25 to 280 °C; the sample powder (ca. 10 mg) was sandwiched in the middle of Al sheet with single cantilever bending mode. TEM images were recorded using a JEOL-2100 transmission electron microscope operated at an accelerating voltage of 200 kV.

Py-Bz-T/OBA-POSS/SWCNT Nano-Hybrid Complexes

To prepared Py-Bz-T/OBA-POSS complexes, desired amounts of Py-Bz-T and OBA-POSS were dissolved in THF and stirred for 2 h at room temperature and them concentrated under a flow of N_2 at room temperature for 8 h. The nanocomposite was placed in a vacuum oven at 100 °C for 12 h. To prepare Py-Bz-T/OBA-POSS/SWCNT nano-hybrid complexes, desired amounts of Py-Bz-T and OBA-POSS were dissolved in THF and stirred for 2 h at room temperature. A desired amount of a solution of SWCNTs in THF was added and then the mixed was subjected to ultrasonication for 1 h. The solution of the nano-hybrid complex was concentrated under a flow of N_2 at room temperature for 8 h.

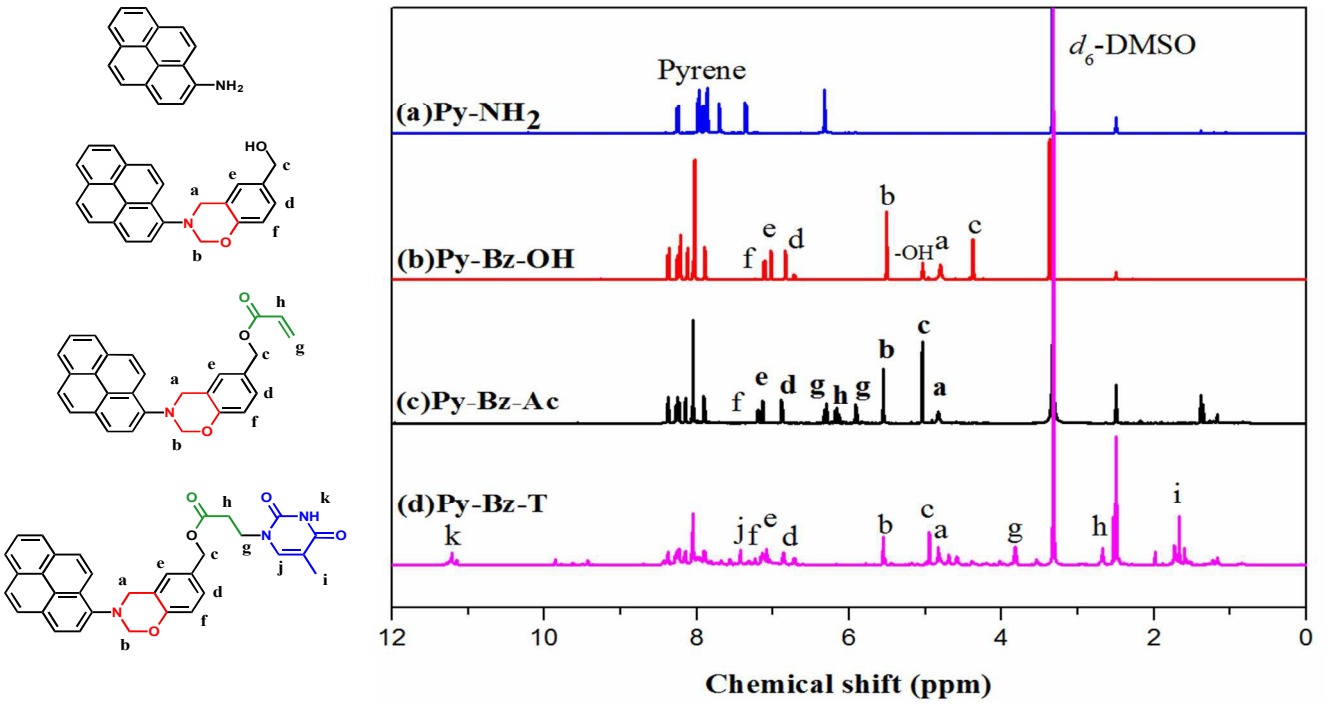

Figure 1: ^{1}H NMR spectra of Py-NH_2, Py-Bz-OH, Py-Bz-Ac, and Py-Bz-T in d_6-DMSO

The residue was placed in a vacuum oven at 100 °C for 12 h. All nanocomposites were thermally polymerized in a stepwise manner: at 110 °C for 4 h, 160 °C for 3 h, 180 °C for 2 h, and 200 °C for 1 h. Each cured sample had a dark brown-red color.

Results and Discussion

Synthesis of Py-Bz-T

Scheme 1 presents the synthesis of Py-Bz-T. We first synthesized Py-Bz-OH through a Mannich reaction from pyren-1-amine (Py-NH_2), formaldehyde, and 4-hydroxybenzyl alcohol. We then esterified Py-Bz-OH with acryloyl chloride at room temperature to give Py-Bz-Ac, featuring an α,β-unsaturated ester (acrylate) functional group that allowed Michael addition of the acetamide group of T to obtain the target compound Py-Bz-T, presenting T and Py moieties at opposite ends of the benzoxazine unit (The detailed synthesis procedures were summarized in supplementary information). We confirmed the chemical structures of Py-Bz-OH, Py-Bz-Ac, and Py-Bz-T using ^{1}H NMR, ^{13}C NMR, and FTIR spectroscopy.

Figures 1 and 2 display the ^{1}H and ^{13}C NMR spectra, respectively, of Py-NH_2, Py-Bz-OH, Py-Bz-Ac, and Py-Bz-T in d_6-DMSO. The signals in Figures 1(a) and 2(a) are consistent with those reported previously.[83] The signals of Py-Bz- OH [Figure 1(b)] at 4.80 and 5.49 ppm represent the protons of its benzoxazine ring. Because Py affected the chemical environment, the difference in chemical shift between these two peaks (0.69 ppm) is smaller than that typically found for benzoxazines.[83] The peak height was also affected by the presence of the Py unit; nevertheless, the ratio of these two integrated peaks was 1:1 (Figure S1). The signals of Py-Bz-OH [Figure 1(b)] at 4.37 and 5.04 ppm represent the protons on the benzylic carbon and OH groups, respectively. Esterification on the OH group caused the proton at benzylic position to move downfield (from 4.37 to 5.02 ppm), while the signal of the OH group disappeared [Figure 1(c)]. The signals of the protons of the α,β-unsaturated C=O group appeared as three doublets of doublets at 5.88, 6.35, and 6.16 ppm. Michael addition to the α,β-unsaturated C=O group caused the signals of these protons to move upfield to 2.67 and 3.83 ppm (O=CCH_2CH$_2$N and O=CCH$_2$CH_2N, respectively) [Figure 1(d)]; the signals of the protons of the T unit were all well defined, consistent with the successful preparation of Py-Bz-T.

The ^{13}C NMR spectrum of Py-Bz-OH [Figure 2(b)] featured signals at 52.18 and 82.07 ppm, corresponding to the carbon nuclei of the benzoxazine ring (CCH$_2$N, NCH$_2$O), and 62.84 ppm, corresponding to the carbon nuclei of the benzylic group. The signal of the benzylic carbon nuclei moving downfield slightly to 65.2 ppm after esterification [Figure 2(c)], with a signal appearing for the C=O group at 166.19 ppm. The ^{13}C NMR spectrum of Py-Bz-T featured signals at 32.92 and 43.95 ppm, corresponding to the carbon nuclei O=CCH$_2$CH$_2$N and O=CCH$_2$CH$_2$N, respectively [Figure 2(d)]; again, the signals of the carbon nuclei of the T unit were all well defined, confirming the success of the Michael addition. Figure 3 presents the FTIR spectra of Py-NH_2, Py-Bz-OH, Py-Bz-Ac, and Py-Bz-T. The characteristic absorption bands of Py-Bz-OH appeared at 942 and 1240 cm^{-1} for the benzoxazine ring out-of-plane C–H bending and the benzoxazine ring ether stretching, respectively [Figure 3(b)]. The characteristic absorption bands of Py-Bz-OH appeared at 1604 cm^{-1}, for the aromatic C–C stretching, and near 3400 cm^{-1}, for the OH group. After esterification [Figure 3(c)], the absorption band near 3400 cm^{-1} for the OH group had disappeared, with characteristic absorption bands appearing for the ester at 1180 (ester C–O–C stretching) and 1722 (ester C=O stretching) cm^{-1}. After Michael addition [Figure 3(d)], the characteristic absorption bands for the T group appeared at 1676 (C=O stretching) and 3186 (N–H stretching) cm^{-1}. Overall, the ^{1}H NMR, ^{13}C NMR, and FTIR spectral data confirmed the synthesis of Py-Bz-T and the chemical structures of Py-Bz-OH, Py-Bz-Ac, and Py-Bz-T.

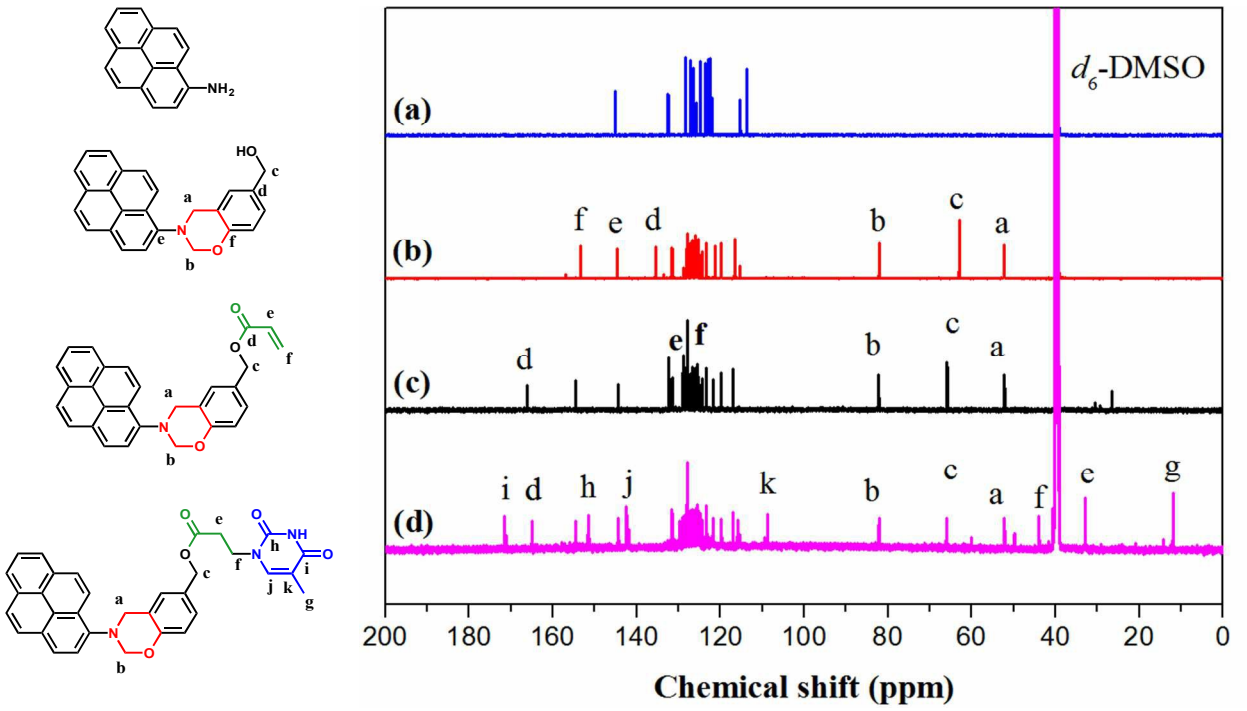

Figure 2: ^{13}C NMR spectra of Py-NH_2, Py-Bz-OH, Py-Bz-Ac, and Py-Bz-T in d_6-DMSO

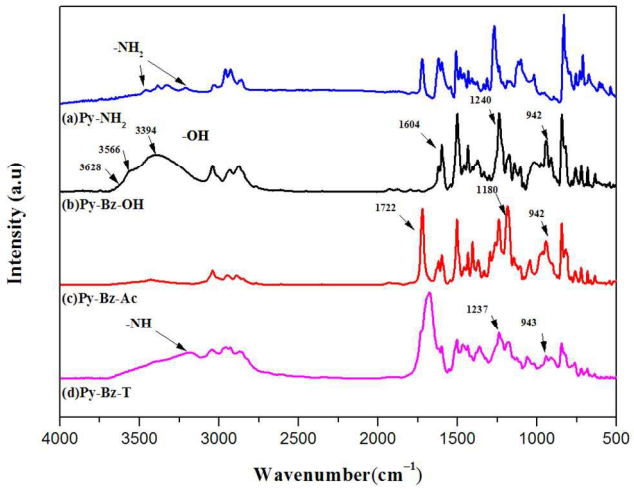

Figure 3: FTIR spectra of Py-NH_2, Py-Bz-OH, Py-Bz-Ac, and Py-Bz-T

Thermal Properties of Py-Bz-T

We performed DSC and TGA analyses of Py-Bz-OH, Py-Bz-Ac, and Py-Bz-T from 35 to 300 °C at a heating rate of 20 °C min^{-1} under a N_2 atmosphere (Figures S2 and S3). The presence of the T unit in Py-Bz-T led to a dramatic decrease in the curing temperature as a result of increasing the concentration of oxonium ions in the medium. To investigate the polymerization behavior of Py-Bz-T, Figure 4 presents DSC thermograms and FTIR spectra of the pure Py-Bz-T monomer recorded after heating at various temperatures. The DSC curve [Figure 4(a)] of the uncured Py-Bz-T featured a glass transition temperature (T_g) at 90 °C, suggesting aggregation of Py units and multiple T···T hydrogen bonding interactions,[19,23,89,90] and an exothermic peak with a maximum at 226 °C and a reaction heat of 122 J g^{-1}. After thermal curing at 110 °C for 4 h and cooling to room temperature, the DSC thermogram curve of Py-Bz-T was similar to that of the uncured Py-Bz-T. The value of T_g increased slightly to 105 °C while the reaction heat of the exothermic peak decreased slightly to 113 J g^{-1}. After thermal curing at 160 °C for 3 h, however, the glass transition temperature increased to 124 °C and the exothermic peak of the polymerization reaction slightly decreased with a maximum at 224 °C and a reaction heat of 109 J g^{-1}. After thermal curing at 180 °C for 2 h, the value of T_g increased to 139 °C and the exothermic peak of the polymerization reaction nearly disappeared completely (Figure S4). Moreover, the value of T_g was higher (170 °C) after curing at higher thermal curing temperatures (200 °C for 1 h), and the exothermic peak of the polymerization reaction remaining absent. Therefore, our sample of Py-Bz-T underwent polymerization through simple thermal curing process in a stepwise manner without any catalyst; the cured poly(Py-Bz-T) exhibited a very high glass transition temperature, suggesting great thermal stability.

We used FTIR spectroscopy [Figure 4(b)] to characterize the structures formed from Py-Bz-T at the various heating stages to further characterize the thermal curing process of polymerization. The intensities of the characteristic absorption bands of Py-Bz-T at 942 and 1240 cm^{-1}, representing C–H bending and ether stretching of the benzoxazine ring, decreased slightly after heating at 160 °C. In contrast, these characteristic absorptions at 942 cm^{-1} disappeared completely after heating at 200 °C, suggesting that ring-opening polymerization of the Py-Bz-T monomer was complete. Thus, the FTIR spectra of Py-Bz-T recorded after the various heating stages were consistent with the DSC thermograms.

We also used TGA, performed from 35 to 800 °C at a heating rate of 20 °C min^{-1} under a N_2 atmosphere, to investigate the thermal properties of Py-Bz-OH, Py-Bz-Ac, and Py-Bz-T (Figure S3). The thermal stability of Py-Bz-T [Figure S3(c)] was

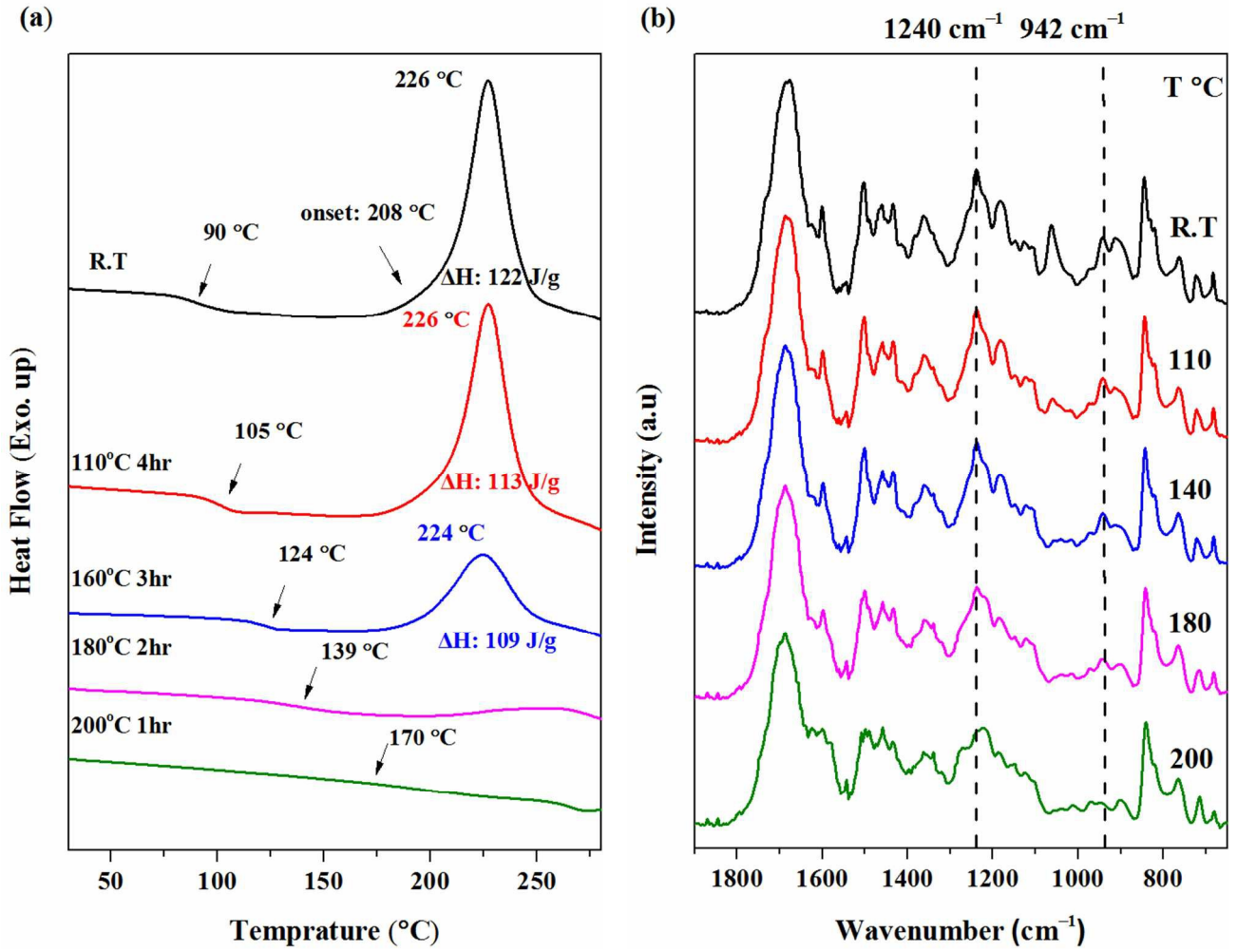

Figure 4: (a) DSC thermograms and (b) FTIR spectra of Py-Bz-T, recorded after various stages of high-temperature curing

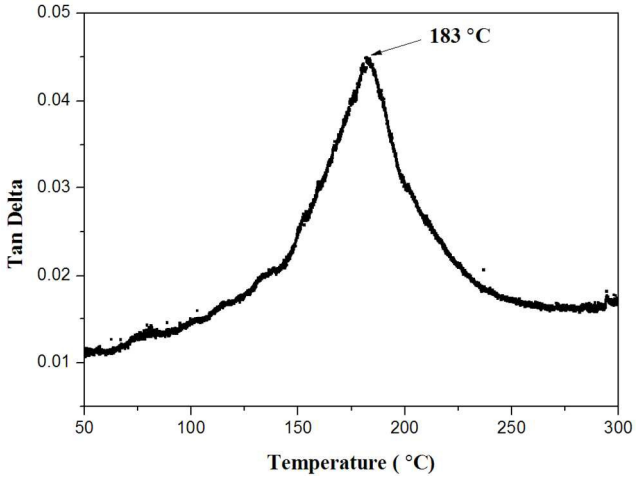

Figure 5: DMA analysis of cured Py-Bz-T

characterized by a decomposition temperature required for 5 wt % loss (T_d) of 220 °C and a char yield of 37.6%; the cured poly(Py-Bz-T) exhibited a value of T_d of 304 °C and a char yield of 44.6%. The thermal stabilities increased after thermal curing of all of the benzoxazine compounds in this study (Figure S3). In addition, we used DMA to further investigate the thermal properties of cured Py-Bz-T. The value of T_g of cured Py-Bz-T determined using DMA was 183 °C, obtained from the maxima of the tan □ plots in Figure 5. Although the value of T_g obtained through DMA analysis was higher than that from the DSC analysis (presumably because of their different measurement principles), our DSC, TGA, and DMA analyses confirmed that poly(Py-Bz-T) possessed great thermal stability.

Self-Assembly and Thermal Properties of Py-Bz-T/OBA-POSS Nanocomposites

We prepared OBA-POSS according to a previously reported procedure[84] and characterized its chemical structure using ^{1}H NMR, ^{13}C NMR, and FTIR spectroscopy (Figure S5). We employed ^{1}H NMR and FTIR spectroscopy to investigate the intermolecular hydrogen bonding in the Py-Bz-T/OBA-POSS nanocomposites. While increasing the OBA-POSS concentration from 50 to 90 wt % and pure Py-Bz-T, we recorded ^{1}H NMR spectra (25 °C; tetrachloroethane-d_2) to characterize the association constants (K_a) of the hydrogen-bonded complexes. The signal of the T imide unit of Py-Bz-T shifted downfield upon increasing the concentration of OBA-POSS (Figure 6), moving from 8.62 initially to 10.13 ppm at 50 wt % of OBA-POSS. We used the Benesi–Hildebrand method,[26] from the changes in

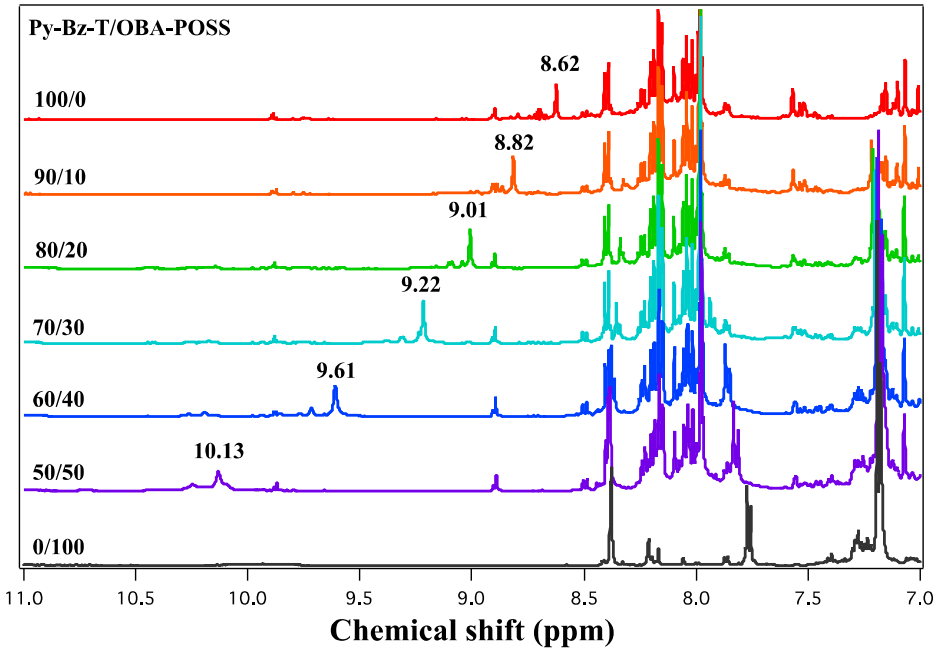

Figure 6: ^{1}H NMR spectroscopic titration of Py-Bz-T/OBA-POSS nanocomposite (amide region of Py-Bz-T)

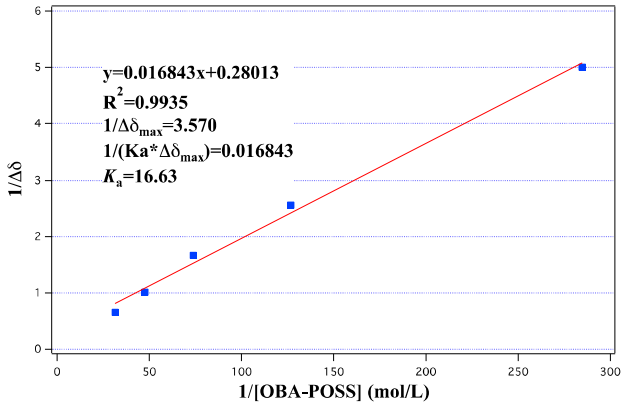

Figure 7: Benesi–Hildebrand plots and fitting data for T···A association in d_2-tetrachloroethane at 25 °C

chemical shift ($\Delta\delta$) and the molar concentration of OBA-POSS, to calculate the value of K_a of the hydrogen-bonded complexes (Figure 7)

$$\frac{1}{\Delta\delta} = \frac{1}{(K_a \Delta\delta_{max}[\text{OBA-POSS}])} + \frac{1}{\Delta\delta_{max}}$$

The value of K_a of Py-Bz-T/OBA-POSS nanocomposite, obtained from the fitting, was around 17 M^{-1}, confirming that A···T hydrogen bonding interactions were present in this nanocomposite, consistent with previous reports.[85, 86]

Infrared spectroscopy is a common tool for investigating multiple hydrogen bonding interactions in the bulk state. We recorded FTIR spectra of Py-Bz-T/OBA-POSS nanocomposites of various weight ratios using the conventional KBr disk method. Figure 8(a) presents the FTIR spectra in N–H stretching vibrational region. The spectrum of OBA-POSS features absorption bands at 3302 and 3130 cm^{-1} representing the N–H stretching of the free and hydrogen-bonded A units, respectively. Similarly, the spectrum of Py-Bz-T features absorption bands at 3184 and 3041 cm^{-1} representing the N–H stretching of hydrogen-bonded and free T moieties, respectively. In contrast, the FTIR spectra of Py-Bz-T/OBA-POSS nanocomposites prepared at different weight ratios all featured three absorption bands, with the N–H stretching band for hydrogen-bonded A···T units having shifted to near 3186 cm^{-1}. The absorption band at 3331 cm^{-1} represented free N–H stretching from OBA-POSS; its absorption intensity increased upon increasing the concentration of OBA-POSS. The broad absorption band around 3200 cm^{-1} represented free N–H stretching from Py-Bz-T; its absorption intensity decreased upon increasing the concentration of OBA-POSS. Figure 8(b) presents the double bond stretching vibrational region of the FTIR spectra. The spectrum of Py-Bz-T features a main absorption band near 1670 cm^{-1}, arising from stretching of both free and hydrogen-bonded C=O units, as well as a small absorption at 1600 cm^{-1} representing C=C stretching. The spectrum of OBA-POSS featured bands near 1660 and 1604 cm^{-1}, representing adenine ring stretching of hydrogen-bonded and free plus NH_2 moieties, respectively.[89] Accordingly, we used the second derivative technique to analyze the FTIR spectra of these Py-Bz-T/OBA-POSS nanocomposites prepared at different weight ratios, examining the behavior of the three major absorption signals near 1700, 1670, and 1600 cm^{-1} (Figure S6). The main absorption band near 1670 cm^{-1} represented the stretching of multiple-hydrogen-bonded double bonds, including the C=O units involved in T···T and A···T interactions and the C=N units involved in A···T and A···A interactions. Therefore, we focused our calculations based only on the area fractions of the free C=O units of T at 1700 cm^{-1} and the free C=N units of A at 1600 cm^{-1} (Figure 9). The area fraction of the free T group in Py-Bz-T decreased and the area fraction of the free A group in OBA-POSS increased upon increasing the content of OBA-POSS, consistent with the results obtained from the N–H stretching region. Overall, the ^{1}H NMR and FTIR spectra confirmed the existence of multiple hydrogen bonding interactions in the Py-Bz-T/OBA-POSS nanocomposites.

We used DSC to investigate the thermal properties of the Py-Bz-T/OBA-POSS nanocomposite prepared at various weight ratios (Figure 10). We performed these DSC analyses under a N_2 atmosphere, with heating from 35 to 300 °C at a rate of 20 °C min^{-1}; cooling from 300 to 0 °C at a rate 20 °C min^{-1}; isothermal

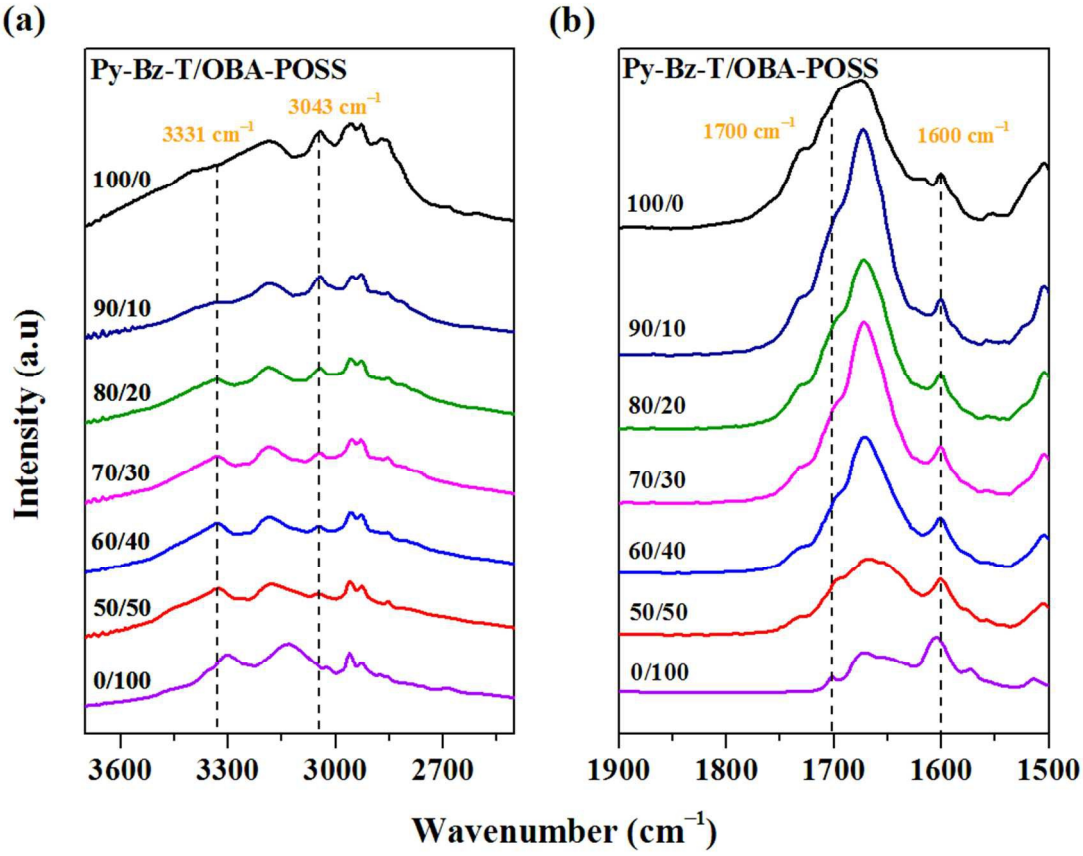

Figure 8: FTIR spectra of Py-Bz-T/OBA-POSS nanocomposites of various weight ratios: (a) 3700–2500 and (b) 1900–1500 cm^{-1} regions

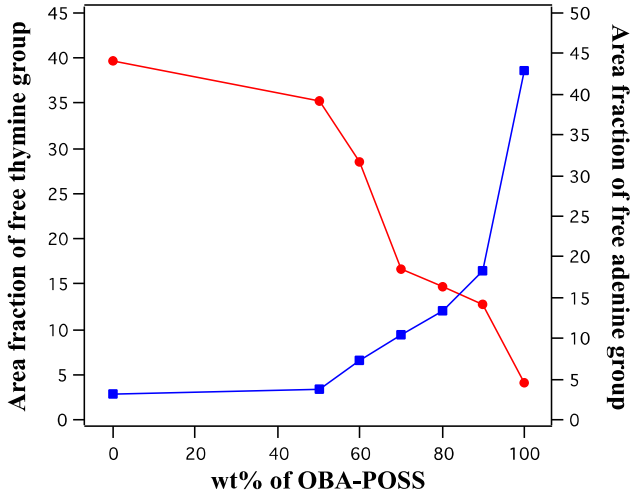

Figure 9: Area fraction analysis of Py-Bz-T/OBA-POSS nanocomposites of various weight ratios

treatment for 1 min; and than heating again to 230 °C in a second heating run. In the first heating run [Figure 10(a)], the DSC trace of OBA-POSS featured two melting peaks at 148 and 164 °C, with Py-BZ-T providing an exothermic peak with a maximum at 226 °C and a reaction heat of 122 J g^{-1}. The exothermic heat energy for benzoxazine ring-opening polymerization decreased from 79 to 12 J g^{-1} upon increasing the concentration of OBA-POSS. We suspect that OBA-POSS was uniformly dispersed in the Py-Bz-T/OBA-POSS nanocomposite, due to the hydrogen bonding interactions, thereby obstructing the polymerization of Py-Bz-T monomers and decreasing the degree of polymerization. In the second heating run [Figure 10(b)], the DSC traces of none of the Py-Bz-T/OBA-POSS nanocomposite featured an exothermic peak near 220 °C, suggesting that the ring-opening polymerization of Py-Bz-T was complete during the first heating run. The values of T_g of the Py-Bz-T/OBA-POSS nanocomposites in the second heating run increased from 50 to 164 °C upon increasing the concentration of Py-Bz-T. In addition, the single value of T_g and linear relationship between the value of T_g and the OBA-POSS content suggested that the OBA-POSS nanoparticles were dispersed uniformly in the poly(Py-BZ-T) matrix, stabilized through multiple-hydrogen-bonding A···T interactions in the Py-Bz-T/OBA-POSS nanocomposites.

Py-Bz-T/OBA-POSS/SWCNTs Hybrid Complexes

We chose the Py-Bz-T/OBA-POSS nanocomposite formed at a weight ratio of 60/40 (molar ratio of Py-Bz-T to OBA-POSS of 8:1) to investigate the ability to form supramolecular structures from the zero-dimensional POSS nanostructure and the one-dimensional SWCNT nanostructures. We added 1 and 3 wt % of the SWCNTs, with respect to the total weight of the Py-Bz-T/OBA-POSS nanocomposite, into their THF solution. Figure 11 presents photographs of THF solutions of the Py-Bz-T/OBA-POSS nanocomposite (60/40), 1 wt % of SWCNTs in the presence of Py-Bz-T/OBA-POSS, 3 wt % of SWCNTs in the presence of Py-Bz-T/OBA-POSS, and the pure SWCNTs, after they had been left for seven days. The Py-Bz-T/OBA-POSS

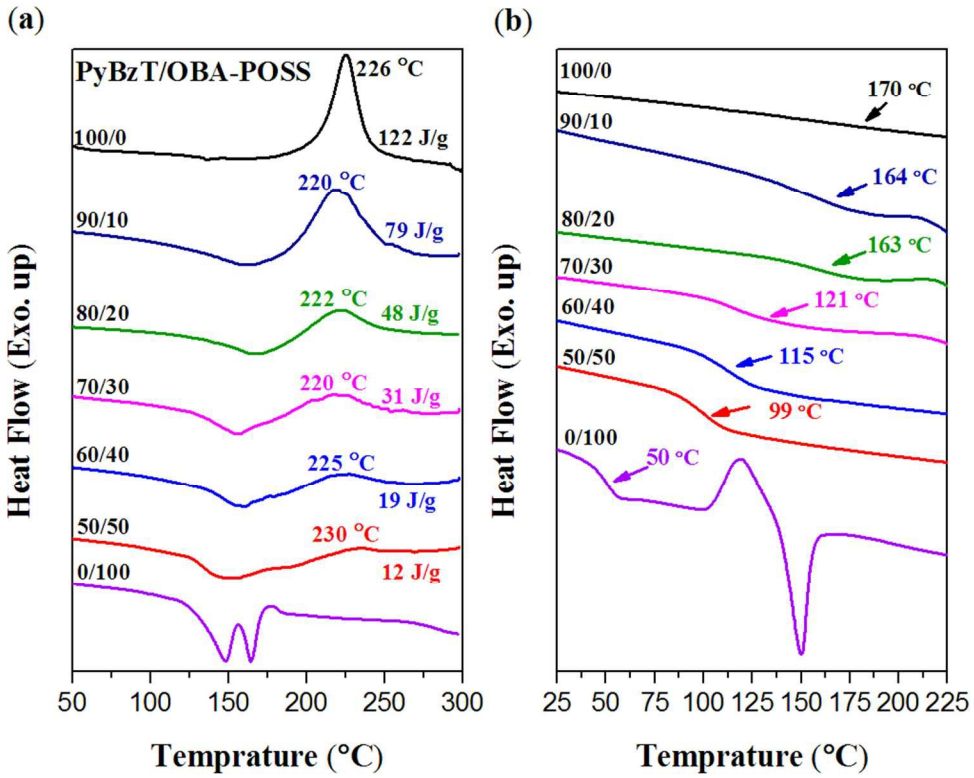

Figure 10: DSC thermograms of the (a) first and (b) second heating runs of Py-Bz-T/OBA-POSS nanocomposites of various weight ratios

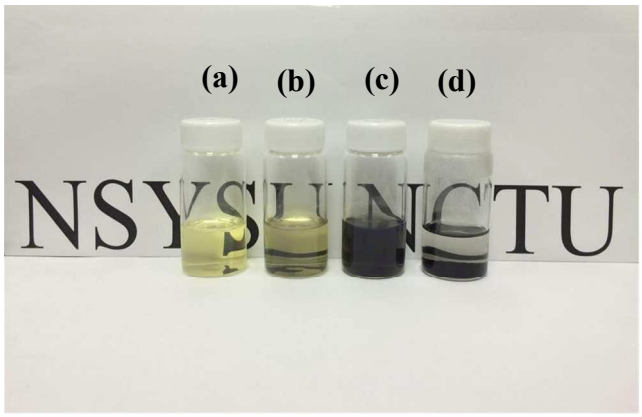

Figure 11 Photographs of THF solutions/suspensions (each 1 mg/mL) of the (a) Py-Bz-T/OBA-POSS nanocomposite (60/40), (b) Py-Bz-T/OBA-POSS/1 wt % SWCNT hybrid complex, (c) Py-Bz-T/OBA-POSS/3 wt % SWCNT hybrid complex, and (d) pristine SWCNTs.

nanocomposite formed a clear yellow solution, whereas the pure SWCNTs precipitated completely. In contrast, the 1 and 3 wt % SWCNTs in the presence of Py-Bz-T/OBA-POSS formed clear dark-yellow and dark-brown solutions, respectively, without any precipitation, suggesting that soluble hybrid complexes had formed that were stabilized through supramolecular interactions. We used TEM to investigate the morphologies of these dispersions of Py-Bz-T/OBA-POSS/SWCNT hybrid complexes in THF (each at 0.1 mg/mL). Self-aggregation of SWCNTs is thermodynamically favored because of van der Waals attraction.

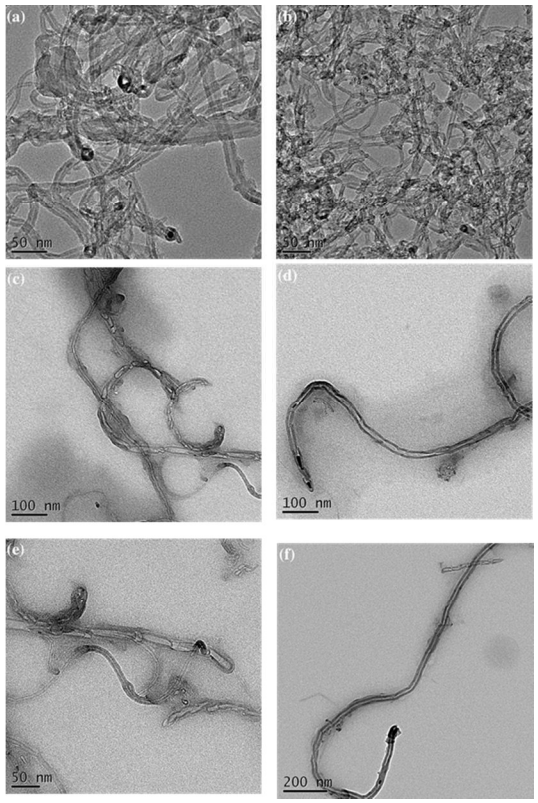

Figure 12 TEM images of the (a, b) pristine SWCNTs, (c, d) Py-Bz-T/OBA-POSS/1 wt % SWCNT hybrid complex, and (e, f) Py-Bz-T/OBA-POSS/3 wt % SWCNTs hybrid complex.

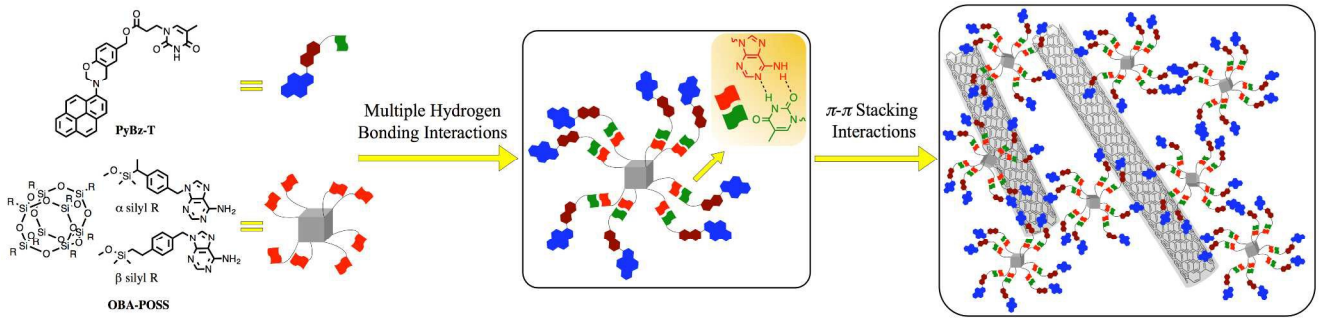

Scheme 2 Cartoon representation of the formation of Py-Bz-T/OBA-POSS/SWCNT hybrid complexes.

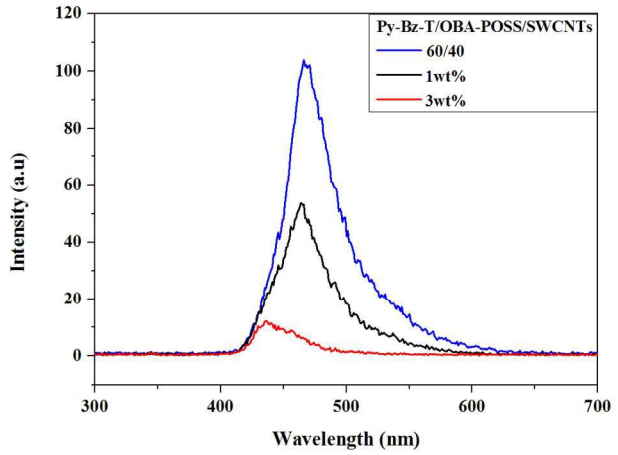

Figure 13 Fluorescence spectra of Py-Bz-T/OBA-POSS/SWCNT hybrid complexes

Figures 12(a) and 12(b) present TEM images of the pristine SWCNTs, which exhibited a high degree of aggregation. Figures 12(c) and 12(d) reveal that the 1 wt % SWCNTs were dispersed uniformly in their Py-Bz-T/OBA-POSS/SWCNT hybrid complex, presumably stabilized through π–π interactions with the Py units. Moreover, the 3 wt % SWCNTs were also dispersed uniformly in their Py-Bz-T/OBA-POSS/SWCNT hybrid complex [Figures 12(e) and 12(f)].

Fluorescence spectroscopy is a useful tool for investigating π–π interactions. The UV–Vis spectrum of the Py-Bz-T/OBA-POSS nanocomposite in THF (concentration of Py-Bz-T: 10^{-2} M) featured an absorption band with the maximum near 346 nm (Figure S7). Thus, we recorded fluorescence spectra (Figure 13) of the Py-Bz-T/OBA-POSS/SWCNT hybrid complexes in THF (concentration of Py-Bz-T: 10^{-2} M) with excitation at 346 nm. The fluorescence spectrum of the Py-Bz-T/OBA-POSS nanocomposite exhibited a strong fluorescence signal at 469 nm, presumably arising from the eximeric Py units. The fluorescence intensity of this signal for the Py-Bz-T/OBA-POSS/SWCNT hybrid complexes decreased upon increasing the amount of SWCNTs, consistent with the Py-Bz-T/OBA-POSS nanocomposite interacting with the SWCNTs through π–π stacking.[87, 88] The fluorescence signal arising after blending with 3 wt % SWCNTs was shifted to 436 nm, suggesting that the Py unit of Py-Bz-T was affected by the steric bulk of the SWCNTs. Therefore, we propose a model for the Py-Bz-T/OBA-POSS/SWCNT hybrid complexes that features SWCNTs covered by Py-Bz-T/OBA-POSS nanocomposites as well as non-interacting Py-Bz-T/OBA-POSS nanocomposites (Scheme 2).

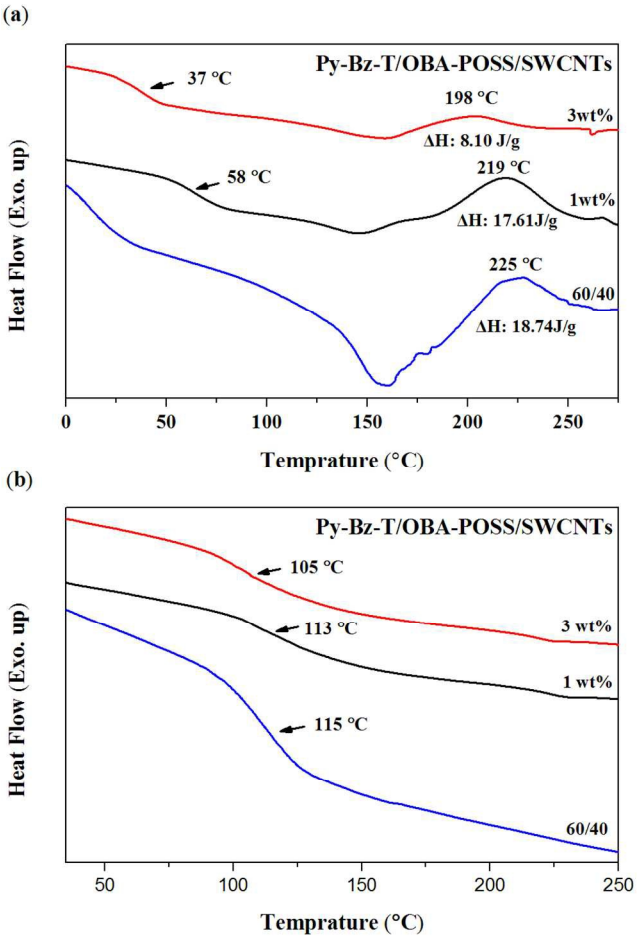

Figure 14 DSC thermograms of the (a) first and (b) second heating runs of Py-Bz-T/OBA-POSS/SWCNT hybrid complexes incorporating various amounts of SWCNTs.

We used DSC to investigate the thermal properties of Py-Bz-T/OBA-POSS/SWCNT hybrid complexes containing different amounts of blended SWCNTs (Figure 14). We performed these DSC analyses under a N_2 atmosphere with a first heating run involving cooling to 0 °C at a rate of 20 °C min^{-1}, isothermal treatment for 1 min, and than heating to 280 °C at a rate of 20 °C min^{-1}, and a second heating run involving cooling from 280 to 0 °C at a rate of 20 °C min^{-1}, isothermal treatment for 1 min, and than heating to 250 °C. In the first heating run, the DSC trace of the pure Py-Bz-T/OBA-POSS (60/40)

View Article Online
DOI: 10.1039/C5SM02559A

nanocomposite featured an exothermic peak with a maximum at 225 °C and a reaction heat of 18.7 J g^{-1} [Figure 14(a)]. The exothermic peak and heat energy for benzoxazine ring-opening polymerization both decreased, from 225 °C and 18.7 J g^{-1} to 198 °C and 8.1 J g^{-1}, respectively, upon increasing the amount of blended SWCNTs, presumably caused mainly by the effect of the steric bulk of the SWCNTs.

As mentioned above, the zero-dimensional nanostructure of OBA-POSS affected the polymerization of the Py-Bz-T monomer, while the fluorescence spectra revealed that the SWCNTs also affected the aggregation of the Py-Bz-T monomer. Accordingly, we believe that the steric bulk of the one-dimensional SWCNT nanostructures also obstructed the polymerization of the Py-Bz-T monomer in the Py-Bz-T/OBA-POSS/SWCNT hybrid complexes. In the second heating run [Figure 14(b)], the DSC traces of none of the Py-Bz-T/OBA-POSS/SWCNT hybrid complexes featured an exothermic peak near 220 °C, suggesting that the ring-opening polymerization of Py-Bz-T was complete during the first heating run. The value of T_g observed in the second heating run decreased slightly, from 115 to 105 °C, upon increasing the amount of blended SWCNTs. The obstructing effect of the steric bulk of the SWCNTs was more pronounced than that of OBA-POSS during the polymerization of the Py-Bz-T monomer in the first heating run. Nevertheless, the degree of the decrease in the value of T_g caused by the SWCNTs was not dramatic because the SWCNTs also limited the free volume (spacing) between the polymer chains. Therefore, the Py-Bz-T/OBA-POSS/SWCNT hybrid complexes maintained their excellent thermal properties.

Conclusions

We have synthesized and characterized a new T-functionalized benzoxazine Py-Bz-T, derived from 1-aminopyrene, that features Py and T moieties at opposite ends of a benzoxazine unit. We investigated the curing behavior and thermal properties of Py-Bz-T, which readily polymerized upon heating at 200 °C for 1 h in the absence of any catalyst. The presence of the T units increased the physical cross-linking density of the polymer. We prepared Py-Bz-T/OBA-POSS nanocomposites and used ^{1}H NMR and FTIR spectroscopy to investigate the multiple hydrogen bonding A···T interactions between Py-Bz-T and OBA-POSS. Such multiple hydrogen bonding interactions and π–π stacking allowed us to prepare Py-Bz-T/OBA-POSS/SWCNT hybrid complexes in THF. Photographic and TEM images revealed that the SWCNTs were highly dispersed in these complexes, covered by the Py-Bz-T/OBA-POSS nanocomposites. Fluorescence spectroscopy confirmed the presence of π–π interactions between Py-Bz-T/OBA-POSS and the SWCNTs in the hybrid complexes.

Acknowledgments

This study was supported financially by the Ministry of Science and Technology, Taiwan (contracts MOST103-2221-E-110-079- MY3 and MOST102-2221-E-110-008-MY3). We thank Mr. Hsien-Tsan Lin (Regional Instruments Center in National Sun Yat-Sen University) for assistance with the TEM experiments.

Reference:

1. W. J. Burke, *J. Am. Chem. Soc.*, 1949, **71**, 609–612.
2. G. Riess, J. M. Schwob and G. Guth, *Abstr. Pap. Am. Chem. Soc.*, 1984, **188**, 85.
3. H. Schreiber, *German Patent* 2 255 504, 1973.
4. Chernykh, J. P. Liu and H. Ishida, *Polymer*, 2006, **47**, 7664–7669.
5. Kiskan, B. Koz and Y. Yagci, *J. Polym. Sci., Part A: Polym. Chem.*, 2009, **47**, 6955–6961.
6. R. Kudoh, A. Sudo and T. Endo, *Macromolecules*, 2010, **43**, 1185–1187.
7. H. Xu, Z. Lu and G. Zhang, *RSC Adv.*, 2012, **2**, 2768–2772.
8. M. Imran, B. Kiskan and Y. Yagci, *Tetrahedron Lett.*, 2013, **54**, 4966–4969.
9. H. K. Shih, Y. L. Chu, F. C. Chang, C. Y. Zhu and S. W. Kuo, *Polym. Chem.*, 2015, **6**, 6227–6237.
10. N. N. Ghosh, B. Kiskan and Y. Yagci, *Prog. Polym. Sci.*, 2007, **32**, 1344–1391.
11. C. F. Wang, Y. C. Su, S. W. Kuo, C. F. Huang, Y. C. Sheen and F. C. Chang, *Angew. Chem. Int. Ed.*, 2006, **45**, 2248 – 2251.
12. Y. Yagci, B. Kiskan and N. N. Ghosh, *J. Polym. Sci., Part A: Polym. Chem.*, 2009, **47**, 5565-5576.
13. M. R. Vengatesan, S. Devaraju, K. Dinakaran and M. Alagar, *J. Mater. Chem.*, 2012, **22**, 7559-7566.
14. C. F. Wang, S. F. Chiou, F. H. Ko,J.K. Chen, C. T. Chou, C. F. Huang, S. W. Kuo and F. C. Chang, *Langmuir*, 2007, **23**, 5868–5871.
15. C. F. Wang, F. C. Chang and S. W. Kuo, *Hand book of polybenzoxazine Resins*, 2011, **33**, p. 579.
16. T. Agag, S. Geiger and H. Ishida, *Hand book of polybenzoxazine Resins*, 2011, **13**, p. 263.
17. J. Dunkers, E. A. Zarate and H. Ishida, *J. Phys. Chem.*, 1996, **100**, 13514−13520.
18. H.-D. Kim and H. Ishida, *J. Phys. Chem. A*, 2002, **106**, 3271− 3280.
19. L. Brunsveld, B. J. B. Folmer, E. W. Meijer and R. P. Sijbesma, *Chem. Rev.*, 2001, **101**, 4071–4097.
20. J. L. Sessler, C. M. Lawrence and J. Jayawickramarajah, *Chem. Soc. Rev.*, 2007, **36**, 314–325.
21. C. Richard, F. Balavoine, P. Schultz, T. W. Ebbesen and C. Mioskowski, *Science*, 2003, **300**, 775–778.
22. H. Lin, C. C. Cheng, Y. C. Yen and F. C. Chang, *Macromolecules*, 2010, **43**, 1245–1252.
23. H. Wang, O. Altukhov, C. C. Cheng, F. C. Chang and S. W. Kuo, *Soft Matter*, 2013, **9**, 5196–5206.
24. J. Goshe, I. M. Steele, C. Ceccarelli, A. L. Rheingold and B. Bosnich, *Proc. Natl. Acad. Sci. U. S. A.*, 2002, **99**, 4823–4829.
25. M. J. Rashkin and M. L. Waters, *J. Am. Chem. Soc.*, 2002, **124**, 1860–1861.
26. S. Sivakova and S. J. Rowan, *Chem. Soc. Rev.*, 2005, **34**, 9–21.
27. W. H. Binder and R. Zirbs, *Adv. Polym. Sci.*, 2007, **207**, 1–78.
28. B. J. B. Folmer, R. P. Sijbesma, R. M. Versteegen, J. A. J. van der Rijt and E. W. Meijer, *Adv. Mater.*, 2000, **12**, 874–878.
29. T. F. A. De Greef, M. M. J. Smulders, M. Wolffs, A. P. H. J. Schenning, R. P. Sijbesma and E. W. Meijer, *Chem. Rev.*, 2009, **109**, 5687–5754
30. T. Aida, E. W. Meijer and S. I. Stupp, *Science*, 2012, **335**, 813–817.
31. P. A. Korevaar, S. J. George, A. J. Markvoort, M. M. J. Smulders, P. A. J. Hilbers, A. P. H. J. Schenning, T. F. A. De Greef and E. W. Meijer, *Nature*, 2012, **481**, 492–496.
32. D. Philp and J. F. Stoddart, *Angew. Chem., Int. Ed. Engl.*, 1996, **35**, 1155–1196.
33. Ciferri, *Supramolecular Polymers*, 2nd edn, Taylor and Francis, Boca Raton, Florida, 2005.
34. J. Pedersen, *J. Am. Chem. Soc.*, 1967, **89**, 7017–7036.
35. J. Cram and J. M. Cram, *Science*, 1974, **183**, 803–809.

36. B. Dietrich, J. M. Lehn and J. P. Sauvage, *Tetrahedron Lett.*, 1969, **34**, 2889–2892.
37. E. Sielcken, M. M. van Tilborg, M. F. M. Roks, R. Hendriks, W. Drenth and R. J. M. Nolte, *J. Am. Chem. Soc.*, 1987, **109**, 4261–4265.
38. R. Meissner, X. Garcias, S. Mecozzi, and J. Rebek, Jr., *J. Am. Chem. Soc.*, 1997, **119**, 77–85.
39. D. N. Reinhoudt and M. Crego-Calama, *Science*, 2002, **295**, 2403–2407.
40. R. Sakai, T. Satoh, R. Kakuchi, H. Kaga and T. Kakuchi, *Macromolecules*, 2003, **36**, 3709–3713.
41. G. Yu, M. Xue, Z. Zhang, J. Li, C.u Han and F. Huang, *J. Am. Chem. Soc.*, 2012, **134**, 13248−13251.
42. L. Atwood, J. E. D. Davies, D. D. MacNicol and F. Vögtle, Eds. *Comprehensive Supramolecular Chemistry*, Elsevier Science, Oxford, 1996.
43. J. Prins, D. N. Reinhoudt, P. Timmerman, *Angew. Chem. Int. Ed.*, 2001, **40**, 2382–2426.
44. D. H. Williams, C. T. Calderone, D. P. O'Brien and R. Zerella, *Chem. Commun.*, 2002, 1266–1267.
45. W. L. Jorgensen and J. Pranata, *J. Am. Chem. Soc.*, 1990, **112**, 2008–2010.
46. J. Pranata, S. G. Wierschke and W. L. Jorgensen, *J. Am. Chem. Soc.*, 1991, **113**, 2810–2819.
47. F. Goodman, *Nature*, 1995, **378**, 237–238.
48. E. M. Todd, J. R. Quinn, T. Park and S. C. Zimmerman, *Isr. J. Chem.*, 2005, **45**, 381–389.
49. G. Z. Li, L. C. Wang, H. L. Ni and C. U. Pittman, *J. Inorg. Organo-Metal. Polym.*, 2001, **11**, 123–154.
50. H. Xu, S. W. Kuo, J. S. Lee and F. C. Chang, *Macromolecules*, 2002, **35**, 8788–8793.
51. C. F. Huang, S. W. Kuo, F. J. Lin, W. J. Huang, C. F. Wang, W. Y.Chen and F. C. Chang, *Macromolecules*, 2006, **39**, 300–308.
52. C. H. Lu, F. C. Chang and S. W. Kuo, *Macromol. Chem. Phys.*, 2010, **211**, 1339–1347.
53. G. Li, L. Wang, H. Ni and C. U. Pittman Jr., *J. Inorg. Organomet. Polym.*, 2001, **11**, 123–154.
54. Sellinger and R. M. Laine, *Macromolecules*, 1996, **29**, 2327–2330.
55. Zhang, F. Babonneau, C. Bonhomme, R. M. Laine, C. L. Soles, H. A. Hristov and A. F. Yee, *J. Am. Chem. Soc.*, 1998, **120**, 8380–8391.
56. Q. Chen, R. Xu, J. Zhang and D. Yu, *Macromol. Rapid Commun.*, 2005, **26**, 1878–1882.
57. S. Iijima, *Nature*, 1991, **354**, 56–58.
58. Dresselhaus, G. Dresselhaus and P. Avouris, *Carbon Nanotubes: Synthesis, Structure, Properties and Applications*, Eds., Springer, Berlin, 2001.
59. R. H. Baughman, A. A. Zakhidov and W. A. de Heer, *Science*, 2002, **297**, 787–792.
60. D. Qian, E. C. Dickey, R. Andrew and T. Rantell, *Appl. Phys. Lett.*, 2000, **76**, 2868–2870.
61. S. Kumar, T. D. Dang, F. E. Arnold, A. R. Bhattacharyya, B. G. Min, X. Zhang, R. A. Vaia, C. Park, W. W. Adams, R. H. Hauge, R. E. Smalley, S. Ramesh and P. A. Willis, *Macromolecules*, 2002, **35**, 9039–9043.
62. H. Geng, R. Rosen, B. Zheng, H. Shimoda, L. Fleming, J. Liu and O. Zhou, *Adv. Mater.*, 2002, **14**, 1387–1390.
63. C. Zhang, L. L. Ren, X. Y. Wang and T. X. Liu, *J. Phys. Chem. C*, 2010, **114**, 11435–11440.
64. C. N. R. Rao, B. Satishkumar, A. Govindaraj and M. Nath, *ChemPhysChem*, 2001, **2**, 78–105.
65. D. Tasis, N. Tagmatarchis, A. Bianco, and M. Prato, *Chem. Rev.*, 2006, **106**, 1105−1136.
66. Y. L. Ding, H. Alias, D. S. Wen and R. A. Williams, *Int. J. Heat Mass Transfer*, 2006, **49**, 240–250.
67. A. Balandin, S. Ghosh, W. Bao, I. Calizo, D. Teweldebrhan, F. Miao and C. N. Lau, *Nano Lett.*, 2008, **8**, 902–907.
68. H. Kataura, Y. Kumazawa, Y. Maniwa, I. Umezu, S. Suzuki, Y. Ohtsuka and Y. Achiba, *Synth. Met.*, 1999, **103**, 2555.
69. J.-P. Salvetat, J.-M. Bonard, N. H. Thomson, A. J. Kulik, L. Forro, W. Benoit and L. Zuppiroli, *Appl. Phys. A: Mater. Sci. Process.*, 1999, **69**, 255–260.
70. G. Viswanathan, N. Chakrapani, H. Yang, B.Wei, H. Chung, K. Cho, C. Y. Ryu and P. M. Ajayan, *J. Am. Chem. Soc.*, 2003, **125**, 9258–9259.
71. S. Qin, D. Qin, W. T. Ford, R. E. Resasco and J. E. Herrera, *Macromolecules*, 2004, **37**, 752–757.
72. Y. Yao, W. Li, S. Wang, D. Yan and X. Chen, *Macromol. Rapid Commun.*, 2006, **27**, 2019–2025.
73. A. Hirsch, *Angew. Chem. Int. Ed.*, 2002, **41**, 1853–1859.
74. D. Tasis, N. Tagmatarchis, A. Bianco and M. Prato, *Chem. Rev.*, 2006, **106**, 1105–1136.
75. S. Huang, H. D. Peng, W. W. Tjiu, Z. Yang, H. Zhu, T. Tang and T. X. Liu, *J. Phys. Chem. B*, 2010, **114**, 16766–16772.
76. C. Zhang, W. W. Tjiu, T. X. Liu, W. Y. Lui, I. Y. Phang and W. D. Zhang, *J Phys. Chem. B*, 2011, **115**, 3392–3399.
77. Y. Yang, L. Ren, C. Zhang, S. Huang and T. Liu, *Appl. Mater. Interfaces*, 2011, **3**, 2779–2785.
78. D. Chen, R. Wang, W. W. Tjiu and T. Liu, *Composites Science and Technology*, 2011, **71**, 1556–1562.
79. C. Zhang, S. Huang, W. W. Tjiu, W. Fana and T. Liu, *J. Mater. Chem.*, 2012, **22**, 2427–2434.
80. M. K. Liu, C. Zhang, W. W. Tjiu, Z. Yang, W. Z. Wang and T. X. Liu, *Polymer*, 2013, **54**, 3124–3130.
81. M. K. Liu, W. W. Tjiu, J. S. Pan, C. Zhang, W. Gao and T. X. Liu, *Nanoscale*, 2014, **6**, 4233–4242.
82. M. Liu, Y. Du, Y.-E Miao, Q. Ding, S. He, W. W. Tjiu, J. Pan and Tianxi Liu, *Nanoscale*, 2015, **7**, 1037–1046.
83. M. G. Mohamed, C. H. Hsiao, F. L. Luo, L. Z. Dai and S. W. Kuo, *RSC Adv.*, 2015, **5**, 45201–45212.
84. W. H. Hu, K. W. Huang, C. W. Chiou and S. W. Kuo, *Macromolecules*, 2012, **45**, 9020−9028.
85. L. Fielding, *Tetrahedron*, 2000, **56**, 6151–6170.
86. H. Lin, C. C. Cheng, Y. C. Yen and F. C. Chang, *Macromolecules*, 2010, **43**, 1245–1252.
87. Chen, H. Liu, W.A. Weimer, M.D. Halls, D.H. Waldeck and G.C. Walker, *J. Am. Chem. Soc.*, 2002, **124**, 9034–9035.
88. H. Murakami, T. Nomura and N. Nakashima, *Chem. Phys. Lett.*, 2003, **378**, 481–485.
89. Y. C. Wu and S. W. Kuo, *J. Mater. Chem.*, 2012, **22**, 2982–2991.
90. Y. S. Wu, Y. C. Wu and S. W. Kuo, *Polymers*, 2014, **6**, 1827–1845.

View Article Online
DOI: 10.1039/C5SM02569A

Graphic Abstract

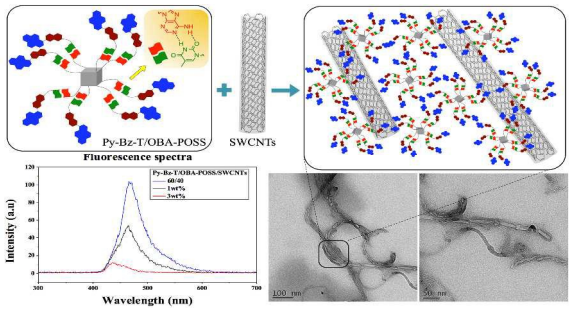

Zero-dimensional POSS with one-dimensional SWCNTs as dual-dimensional nanohybrid complexes within polybenzoxazine matrices stabilized through noncovalent supramolecular interactions.